

# Barium Ion Cooling Simulation

Lukas Mouton  
Semester Project

Supervisors  
Dr. M. Grau & Prof. Dr. J. Home  
Trapped Ion Quantum Information Group, ETH Zürich

31.05.2021

## Abstract

This report is on the construction of a model which simulates the brightness of the most common isotopes of  $\text{Ba}^+$  when two lasers address the  $6s\ ^2S_{1/2} - 6p\ ^2P_{1/2}$  and  $5d\ ^2D_{3/2} - 6p\ ^2P_{1/2}$  transitions. With the model, I reproduce previous results and make new predictions about the brightness of  $\text{Ba}^+$  isotopes. The model produces fits to fluorescence data that I took from an ion trap. Even though the fits look qualitatively good, some of the parameters vary from fit to fit and depend highly on the initial guess of the parameters.

## Acknowledgements

A special thank you goes to my first supervisor Dr. Matthew Grau for guiding me throughout this semester project in a manner that allowed me to reflect on the next steps and get a taste of what research is like, while making sure that I do not wander astray. I also thank Prof. Dr. Jonathan Home for welcoming me in the Trapped Ion Quantum Information Group. Finally, I would like to express my gratitude to Dr. Ilya Sergachev, whose indispensable help in loading and operating the ion trap made parts of this work possible, and Albert Mitjans, whose software tool allowed me to take measurements of the ions' brightness.

## Contents

<b>1</b>	<b>Introduction</b>	<b>3</b>
<b>2</b>	<b>Theory</b>	<b>5</b>
2.1	Master Equation . . . . .	5
2.2	Hamiltonian . . . . .	5
2.2.1	Zeeman Splitting . . . . .	6
2.2.2	Hyperfine Structure . . . . .	8
2.3	Collapse Operators . . . . .	8
2.3.1	Zeeman Splitting . . . . .	8
2.3.2	Hyperfine Structure . . . . .	9
<b>3</b>	<b>Simulations</b>	<b>10</b>
3.1	Ionisation . . . . .	10
3.2	Reproduction of Previous Results . . . . .	11
3.3	1D Frequency Scans . . . . .	12
3.4	2D Frequency Scans . . . . .	13
<b>4</b>	<b>Ion Trap Data</b>	<b>15</b>
4.1	1D Frequency Scans . . . . .	15
4.2	2D Frequency Scans . . . . .	17
4.3	Intensity Dependent Brightness . . . . .	19
<b>5</b>	<b>Discussion &amp; Conclusion</b>	<b>22</b>
	<b>Bibliography</b>	<b>24</b>

# 1 Introduction

The Trapped Ion Quantum Information Group at ETH Zürich is working together with the Swiss Science Centre Technorama in Winterthur to build an ion trap with the goal of allowing visitors to see the trapped ions ( $\text{Ba}^+$ , ideally  $^{138}\text{Ba}^+$ ) with their bare eyes. The trap has already been assembled and is functional. In order to make the ions fluorescent, two lasers termed the *cooling* and *repump* lasers address the  $6s^2S_{1/2} - 6p^2P_{1/2}$  and  $5d^2D_{3/2} - 6p^2P_{1/2}$  transitions, respectively. Figure 1 shows the above mentioned energy levels of the barium ion.

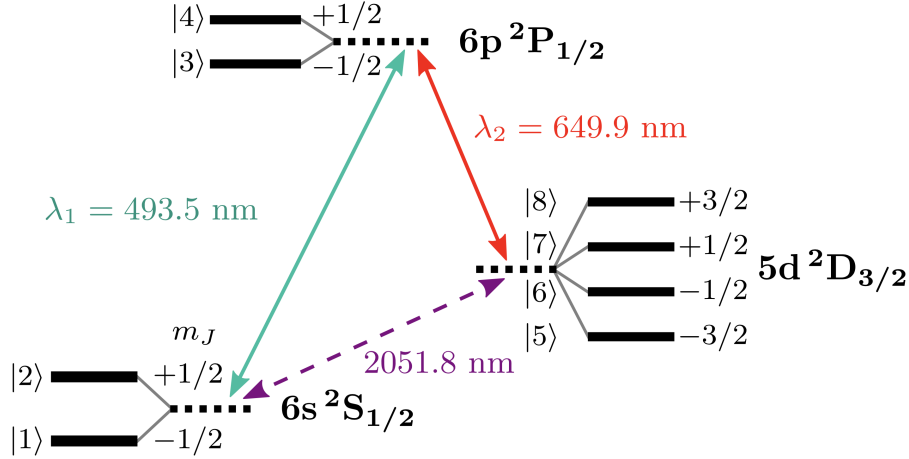


Figure 1: Low-lying energy levels of the  $^{138}\text{Ba}^+$  ion including Zeeman levels (see Section 2). The wavelengths  $\lambda_1$  and  $\lambda_2$  correspond to the frequencies of the cooling and repump lasers on resonance. Figure from [1].

However, occasionally some of the particles in the trap are dark or dimmed, either temporarily or permanently. There are several possibilities why this might happen, such as:

- Different isotopes are in the trap which would not exhibit the same brightness as  $^{138}\text{Ba}^+$  for given laser frequencies, see Section 2.
- The barium ions react with background gas to form molecular ions which do not fluoresce at the same frequencies as  $\text{Ba}^+$ .
- Some ions in the crystal are too far from the point of maximum intensity of the lasers and hence are not equally bright when the laser intensity is below saturation.

Based on data from the ion trap, we would like to be able to gauge various things: what isotopes of  $\text{Ba}^+$  are currently in the trap (or whether it is something else) as well as the values of parameters such as the magnetic field and the laser intensities. To this end, I have constructed an appropriate model in Python.

In previous work, researchers were able to fit a similar model to the brightness of  $\text{Ba}^+$  when targeting the

same energy levels as we do (see Figure 1) with appropriate lasers [1]. They found that the steady-state population of the  $6p\ ^2P_{1/2}$  level can be used to fit the fluorescence of  $Ba^+$ .

This report documents the construction of a model in Python (using the Quantum Toolbox in Python, QuTiP [2]) which is able to estimate the brightness of various isotopes of  $Ba^+$  when addressing the transitions  $6s\ ^2S_{1/2} - 6p\ ^2P_{1/2}$  and  $5d\ ^2D_{3/2} - 6p\ ^2P_{1/2}$  with two lasers (termed  $\nu_1$  and  $\nu_2$ , respectively, in accordance with previous research [1]).

Notice that  $\lambda_1$  in Figure 1 is very close to 498 nm, which is the wavelength at which the rods in the human eye reach their peak receptivity [3]. This is one of the reasons for choosing  $Ba^+$  ions, since the purpose of the ion trap is to allow human observers to directly view the ions in the trap.

In Section 2 I will introduce the theoretical concepts needed to understand how the model calculates the brightness of various  $Ba^+$  isotopes in the trap. In Section 3 I will present the model predictions, followed by my attempts to estimate certain parameters by fitting the model predictions to data from the ion trap in Section 4. Finally, I will review the work in Section 5.

## 2 Theory

In this section, I will make the reader familiar with the theory used in the model. In order to obtain the steady-state population of the  $6p^2P_{1/2}$  level, which can be used to fit the fluorescence of the  $Ba^+$  ion, I shall make use of the quantum mechanical master equation.

### 2.1 Master Equation

The quantum mechanical master equation describes the evolution of a system (i.e. the evolution of its density matrix  $\hat{\rho}$ ) which interacts both coherently and incoherently with an environment [4]. The master equation in Lindblad form is as follows:

$$\frac{d\hat{\rho}}{dt} = -\frac{i}{\hbar}[\hat{H}, \hat{\rho}] + \sum_{\mu} (\hat{L}_{\mu}\hat{\rho}\hat{L}_{\mu}^{\dagger} - \frac{1}{2}\hat{L}_{\mu}^{\dagger}\hat{L}_{\mu}\hat{\rho} - \frac{1}{2}\hat{\rho}\hat{L}_{\mu}^{\dagger}\hat{L}_{\mu}) \quad (1)$$

where  $H$  is the system Hamiltonian and the operators  $\hat{L}_{\mu}$  are the so-called collapse (or jump) operators describing the system's interaction with the environment. The sum is over incoherent processes (indexed by  $\mu$ ) affecting the system. The operators  $\hat{L}_{\mu}$  are normalised according to [5]. A derivation of the master equation in Lindblad form, which also highlights the approximations made along the way, can be found in [5]. One can now already see how to obtain the steady-state population of the  $6p^2P_{1/2}$  level: setting the left hand side of Equation (1) equal to zero and solving for  $\hat{\rho}$ . From there, one can extract the sum of the diagonal elements corresponding to the states in the  $6p^2P_{1/2}$  level. In the remainder of this section I will discuss how to obtain the Hamiltonian  $\hat{H}$  (see Section 2.2) and the collapse operators  $\hat{L}_{\mu}$  (see Section 2.3) for different scenarios (i.e. different kinds of  $Ba^+$  ions).

### 2.2 Hamiltonian

The first term on the right hand side of the master equation includes the system Hamiltonian. As in [1], I shall also make the rotating wave approximation when constructing the Hamiltonian, meaning that I drop terms oscillating at twice the laser frequencies. These terms would average to zero over any reasonable time scale [4]. Constructing the Hamiltonian involves calculating the diagonal terms, which describe the energy levels of the ion, as well as the off-diagonal terms, which describe how the lasers couple the energy levels.

Regarding the energy levels, the reader may recall that there were eight energy levels in Figure 1. This is a consequence of the electron's magnetic moment<sup>1</sup>  $\boldsymbol{\mu}_J$  interacting with a magnetic field (i.e. Earth's magnetic field), leading to a splitting of the energy levels resulting in so-called *Zeeman splitting* [6].

---

<sup>1</sup>I denote vector quantities in bold.

This is the case for all  $\text{Ba}^+$  ions discussed in this report.

Furthermore, the isotopes  $^{137}\text{Ba}^+$  and  $^{135}\text{Ba}^+$  have a nonzero nuclear spin  $\mathbf{I}$ . The interaction between the nuclear spin and the total atomic angular momentum  $\mathbf{J}$  leads to a further splitting of energy levels, resulting in the *hyperfine structure* in these isotopes [7]. The hyperfine constant  $A$  quantifies the size of the hyperfine splitting. Table 1 lists the hyperfine constants which I will make use of in the model.

	$^{137}\text{Ba}^+$	$^{135}\text{Ba}^+$
$6s^2S_{1/2}$	4100 [8]	3590 [9]
$6p^2P_{1/2}$	750 [8]	660 [10]
$5d^2D_{3/2}$	190 [8]	170 [11]

Table 1: Hyperfine splitting constants  $A$  in MHz for the relevant isotopes of  $\text{Ba}^+$  and the states of interest.

An additional reason why the Hamiltonian depends on the isotope of the  $\text{Ba}^+$  ion in question is that the different isotopes experience so-called *isotope shifts* [6]. Different numbers of neutrons in the nucleus cause the transition frequencies between the energy levels to be shifted due to two effects, the mass effect and the volume effect. A detailed discussion of these effects is available in [6]. Table 2 displays the measured isotope shifts as well as the relative abundances of the respective isotopes.

Isotope	$6s^2S_{1/2} - 6p^2P_{1/2}$	$5d^2D_{3/2} - 6p^2P_{1/2}$	Relative Abundance [12]
$^{138}\text{Ba}^+$	0	0	71.7 %
$^{137}\text{Ba}^+$	272 [13]	-13 [10]	11.23 %
$^{136}\text{Ba}^+$	180 [13]	68 [10]	7.85 %
$^{135}\text{Ba}^+$	350 [13]	83 [10]	6.59 %
$^{134}\text{Ba}^+$	223 [13]	175 [10]	2.42 %

Table 2: Isotope shifts and relative abundances for the most common isotopes of  $\text{Ba}^+$ . The isotope shift of  $^m\text{Ba}^+$  is relative to  $^{138}\text{Ba}^+$  ( $\nu_m - \nu_{138}$ ) in MHz.

### 2.2.1 Zeeman Splitting

For the construction of the Hamiltonian in the non-hyperfine case I will follow the derivation in [4].

The full Hamiltonian of the laser-ion system takes the form

$$\hat{H} = \hat{H}_0 + \hat{H}_{\text{int}} \quad (2)$$

where  $\hat{H}_0$  corresponds to the energies of the levels in the ion and  $\hat{H}_{\text{int}}$  describes how they are coupled by the lasers (in a coherent way). In the case where the ions have no hyperfine splitting  $\hat{H}$  will be an  $8 \times 8$  matrix [1]. The Hamiltonians  $\hat{H}_0$  and  $\hat{H}_{\text{int}}$ , after an appropriate rotating frame transformation and the rotating wave approximation, are as follows:

The first part,  $\hat{H}_0$ , is diagonal in the energy basis of the ion:

$$\frac{\hat{H}_{0,ii}}{\hbar} = 2\pi\Delta_l + \delta\omega_i. \quad (3)$$

The detuning  $\Delta_l$  is given by  $\Delta_1 = \nu_1 - \nu_{S-P}$  (for states in the S manifold, as in Figure 1) and  $\Delta_2 = \nu_2 - \nu_{D-P}$  (in the D manifold) where  $\nu_1$  and  $\nu_2$  are the laser frequencies. For states in the P manifold  $\Delta_l = 0$ , due to the rotating frame transformation. The frequency shift  $\delta\omega_i$  stems from the Zeeman splitting and is given by  $\delta\omega_i = g_J\omega_B m_i$  with

$$g_J = 1 + \frac{J(J+1) + S(S+1) - L(L+1)}{2J(J+1)} \quad (4)$$

being the Landé g-factor (with  $J$  the total atomic angular momentum,  $S$  the spin angular momentum and  $L$  the orbital angular momentum),  $\omega_B = \mu_B |\mathbf{B}| / \hbar$  (with  $\mu_B$  the Bohr Magneton) and  $m_i$  the magnetic quantum number [7][1].

The entries in  $\hat{H}_{\text{int}}$ , which are all off-diagonal, are  $\hat{H}_{\text{int},ij} = \Omega_{ij}^0 \sigma_{ij}$  where  $j > i$  (I use the same indexing of the levels as in Figure 1). We can obtain the entries for  $i > j$  by exploiting the fact that  $\hat{H}_{\text{int}}$  is hermitian, i.e. it is equal to its conjugate transpose. The bare (saturation) Rabi frequencies  $\Omega_{ij}^0$  are:

$$\Omega_{ij}^0 = \begin{cases} 2\pi \frac{1}{\sqrt{2}} \Gamma_1 & \text{if } j \text{ and } i \text{ are in the S and P manifold, respectively} \\ 2\pi \frac{1}{\sqrt{2}} \Gamma_2 & \text{if } j \text{ and } i \text{ are in the P and D manifold, respectively} \\ 0 & \text{otherwise} \end{cases} \quad (5)$$

where  $\Gamma_1 = 14.7$  MHz and  $\Gamma_2 = 5.4$  MHz are the partial decay rates [1]. The coefficients  $\sigma_{ij}$  depend on the polarisation of the laser field:

$$\sigma_{ij} = \sqrt{2J_j + 1} \sum_{q=-1}^1 (-1)^{J_i+m_i} \begin{pmatrix} J_i & 1 & J_j \\ -m_i & q & m_j \end{pmatrix} \mathbf{c}_q \cdot \boldsymbol{\epsilon}_l \quad (6)$$

where the brackets denote a Wigner 3j symbol,  $\boldsymbol{\epsilon}_l$  is the polarisation vector of the laser field in question and the vectors  $\mathbf{c}_q$  are:

$$\begin{aligned} \mathbf{c}_1 &= \frac{1}{\sqrt{2}}(-1, i, 0)^T, \\ \mathbf{c}_0 &= (0, 0, 1)^T, \\ \mathbf{c}_{-1} &= \frac{1}{\sqrt{2}}(1, i, 0)^T. \end{aligned} \quad (7)$$

It is worth highlighting that with this choice of the  $\mathbf{c}_q$  I implicitly set the direction of the magnetic field to be along the  $z$ -axis.

The isotope shifts do not affect the partial decay rates  $\Gamma_1$  and  $\Gamma_2$  in a significant way [6]. However, the diagonal entries containing  $\Delta_l$  include the isotope shifts. Consequently, the Hamiltonian will always be influenced by which isotope is in the ion trap, not just by whether the ion spectrum exhibits hyperfine splitting or not.

## 2.2.2 Hyperfine Structure

In the case of the isotopes  $^{137}\text{Ba}^+$  and  $^{135}\text{Ba}^+$ , the hyperfine splitting of the energy levels causes the Hamiltonian to become a  $32 \times 32$  matrix. However, as has been the case so far, the Hamiltonian is still decomposable as in Equation (2). The derivation of the Hamiltonian will be analogous as in Section 2.2.1, but the process becomes more general by introducing the hyperfine quantum number  $\mathbf{F} = \mathbf{J} + \mathbf{I}$ , as done in [7]. Again,  $H_0$  is diagonal, with the entries

$$\frac{H_{0,ii}}{\hbar} = 2\pi\Delta_l + \delta\omega_i + \delta\omega_{\text{hf}} \quad (8)$$

but in contrast to the non-hyperfine case,  $\delta\omega_i = g_F\omega_B m_i$  with

$$g_F = g_J \frac{F(F+1) - I(I+1) + J(J+1)}{2F(F+1)} \quad (9)$$

where  $g_J$  is the Landé g-factor from Equation (4) and the nuclear angular momentum  $I = 3/2$  for  $^{137}\text{Ba}^+$  and  $^{135}\text{Ba}^+$ . The hyperfine energy shift is

$$\delta\omega_{\text{hf}} = 2\pi A \frac{F(F+1) - I(I+1) - J(J+1)}{2} \quad (10)$$

with  $A$  being the hyperfine constant previously encountered in Section 2.2. Regarding the off-diagonal elements of the Hamiltonian, one can again write them as the product  $\hat{H}_{\text{int},ij} = \Omega_{ij}^0 \sigma_{ij}$  with  $\Omega_{ij}^0$  as in Equation (5) but

$$\sigma_{ij} = \sqrt{(2F_i+1)(2F_j+1)(2J_j+1)} \sum_{q=-1}^1 (-1)^{F_i+m_i} \begin{pmatrix} F_i & 1 & F_j \\ -m_i & q & m_j \end{pmatrix} \mathbf{c}_q \cdot \boldsymbol{\epsilon}_l. \quad (11)$$

## 2.3 Collapse Operators

The terms  $L_\mu$  in Equation (1) describe the incoherent spontaneous decay of the ion as well as loss of coherence due to the laser linewidth [4]. As for the Hamiltonian, I will describe how one can calculate the collapse operators for the non-hyperfine case as well as for the hyperfine case.

### 2.3.1 Zeeman Splitting

I will again follow the derivation presented in [4].

The first kind of collapse operator describes spontaneous decay. I introduce an operator for each allowed transition:

$$\hat{c}_{ij} = \sqrt{\Gamma_l \sqrt{2J_j+1}} \begin{pmatrix} J_i & 1 & J_j \\ -m_i & m_i - m_j & m_j \end{pmatrix} |i\rangle \langle j| \quad (12)$$

where  $\Gamma_l$  is the partial decay rate of the transition in question. A transition is allowed when  $\Delta m = 0$  or  $\Delta m = \pm 1$ , with  $\Delta m = 0$  corresponding to the emission of a linearly polarised photon, and  $\Delta m = \pm 1$  corresponding to circular polarisation with opposite handedness [6]. In order to obtain the collapse operator  $\hat{L}_\mu$  I sum all operators which describe the emission of a photon with the same polarisation and energy:

$$\hat{L}_\mu = \sum_{\substack{\Delta m = \text{const.} \\ \Delta E = \text{const.}}} \hat{c}_{ij}. \quad (13)$$

The second kind of collapse operator (also called Markovian dephasing term) accounts for the laser linewidth. I introduce a collapse operator for each laser where the sum goes over all levels which the laser connects to:

$$\hat{L}_\mu = \sum_{l=\text{const.}} \sqrt{\gamma_l} |i\rangle \langle i| \quad (14)$$

where  $\gamma_l$  is the laser linewidth (assuming a Lorentzian profile). Notice, that since the collapse operators only depend on the partial decay rates and the laser linewidth, they are the same for all  $\text{Ba}^+$  isotopes that do not experience hyperfine splitting.

### 2.3.2 Hyperfine Structure

In order to get the collapse operators for the hyperfine case I again turn to [7]. The derivation is analogous to the non-hyperfine case, except that the operators  $\hat{c}_{ij}$  now take the form

$$\hat{c}_{ij} = (-1)^{J_j + I - m_j} \sqrt{\frac{(2J_j + 1)(2F_j + 1)}{2F_i + 1}} \begin{pmatrix} F_j & 1 & F_i \\ m_j & -1 & -m_i \end{pmatrix} \left\{ \begin{matrix} J_j & J_i & 1 \\ F_i & F_j & I \end{matrix} \right\} |i\rangle \langle j| \quad (15)$$

where the curly brackets represent a Wigner 6j symbol. From this point on one can proceed in the same way as in the non-hyperfine case in order to get the collapse operators. As before, the collapse operators do not depend on the isotope in question apart from being different for the hyperfine case.

### 3 Simulations

In this section I will present various simulations that the model produced. In Section 3.1 I will argue why we can expect to find various species of barium isotopes in the trap. Section 3.2 contains plots reproducing the results of previous work and in Sections 3.3 and 3.4 the reader will find new plots of the simulated brightness of barium ions.

#### 3.1 Ionisation

In order to ionise barium the  $6s^2\ ^1S_0 - 6s5d\ ^3D_1$  neutral barium transition is targeted by a 413 nm laser. Due to the motion of the particles, we get Doppler broadening and not all particles see the same laser frequency [14]. Assuming thermal Doppler broadening at 500 °C, meaning the ions' velocities are distributed according to a Maxwell distribution, the transition addressed by the ionisation laser is broadened as seen in Figure 2.

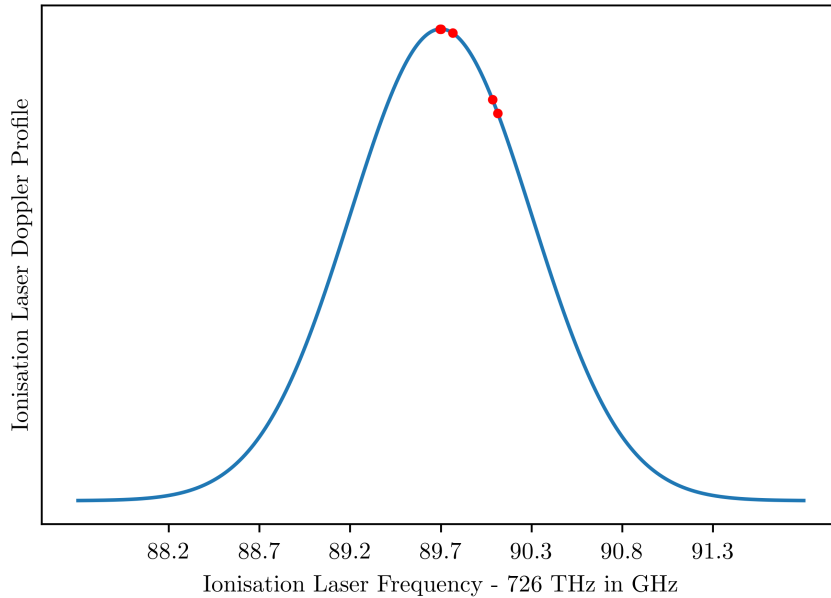


Figure 2: Thermally broadened spectrum of the 413 nm ionisation laser. The red dots indicate the  $6s^2\ ^1S_0 - 6s5d\ ^3D_1$  transition frequencies for the isotopes  $^{138}\text{Ba}^+$  to  $^{134}\text{Ba}^+$ . Isotope shifts from [15]. Note that the transition frequencies for  $^{138}\text{Ba}^+$  and  $^{134}\text{Ba}^+$  are very close together, such that one cannot distinguish two individual dots.

Since the transition frequencies of all the isotope species of  $\text{Ba}^+$  that I consider here are within the range of the broadened laser, one can certainly expect to find other isotopes than  $^{138}\text{Ba}^+$  in the trap.

### 3.2 Reproduction of Previous Results

A first step after having constructed the model was to try and reproduce previous simulations which matched the data such as those in [1]. Figures 3 and 4 aim to reproduce Figures 4 and 5 from [1]. In both graphs, on the  $y$ -axis is the simulated brightness of  $^{138}\text{Ba}^+$  and on the  $x$ -axis is the repump laser frequency  $\nu_2$  which runs over a range of several tens of MHz around resonance. The cooling laser frequency  $\nu_1$  as well as both laser intensities, termed  $I_1$  and  $I_2$  are constant for any given line. The saturation intensities for the transitions of interest are  $I_{1,\text{sat}} = 16.5 \text{ mW cm}^{-2}$  and  $I_{2,\text{sat}} = 2.3 \text{ mW cm}^{-2}$  [16][17].

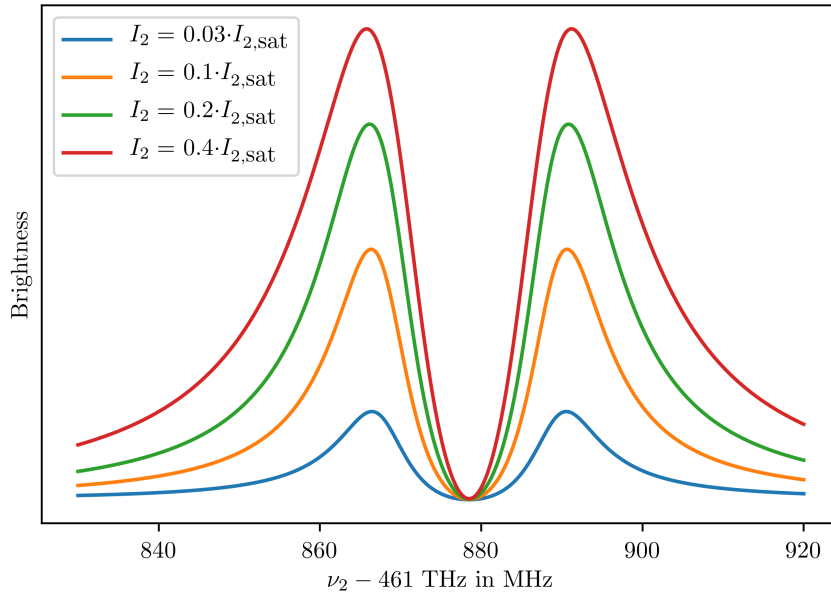


Figure 3: Simulated brightness of  $^{138}\text{Ba}^+$  versus the repump laser frequency  $\nu_2$  for different intensities of the repump laser  $I_2$ . Cooling laser frequency  $\nu_1$  is constant at  $\nu_1 = \nu_{\text{S-P}}$ . Cooling laser intensity  $I_1$  is constant at its saturation intensity. The magnetic field is 0.1 Gauss ( $1 \text{ T} = 10^4 \text{ Gauss}$ ).

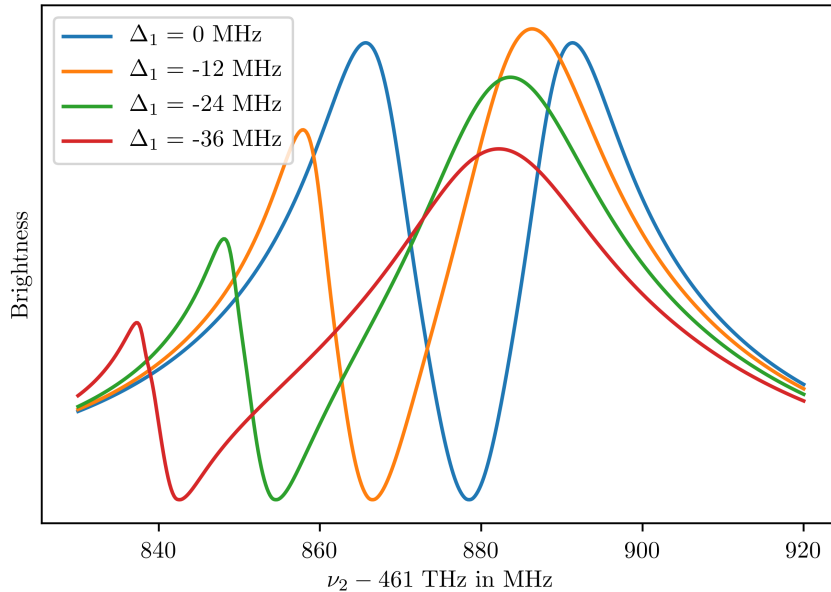


Figure 4: Simulated brightness of  $^{138}\text{Ba}^+$  versus the repump laser frequency  $\nu_2$  for different detunings of the repump laser  $\nu_1$  where  $\Delta_1 = \nu_1 - \nu_{\text{S-P}}$ . Both laser intensities are constant at their respective saturation intensities. The magnetic field is 0.1 Gauss.

Both figures qualitatively match those in [1] well. However, the values of  $I_2$  were ten times larger in [1] than in my model. This might be due to a slightly different definition of the saturation Rabi frequency  $\Omega$  (recall that  $I \propto |\Omega|^2$ ). We use  $\Omega_{\text{sat}} = 2\pi \frac{1}{\sqrt{2}}\Gamma$  as in Equation (5). After having confirmed the ability of the model to generate plots that previous researchers have managed to fit to their data, the next step was to apply it to new domains.

### 3.3 1D Frequency Scans

One of the possible reasons for the particles in the ion trap to be dark or dimmed is that the trap may contain multiple isotopes of  $\text{Ba}^+$ . This not only means that the resonances of some barium ions might be shifted but that their fluorescence spectrum looks qualitatively different, which one can expect to be the case for the ions with hyperfine structure.

In order to get a flavour for how the species of  $\text{Ba}^+$  isotope affects its brightness, Figure 5 shows a similar frequency range of  $\nu_2$  as Figure 3 does but where the different lines correspond to different isotopes.

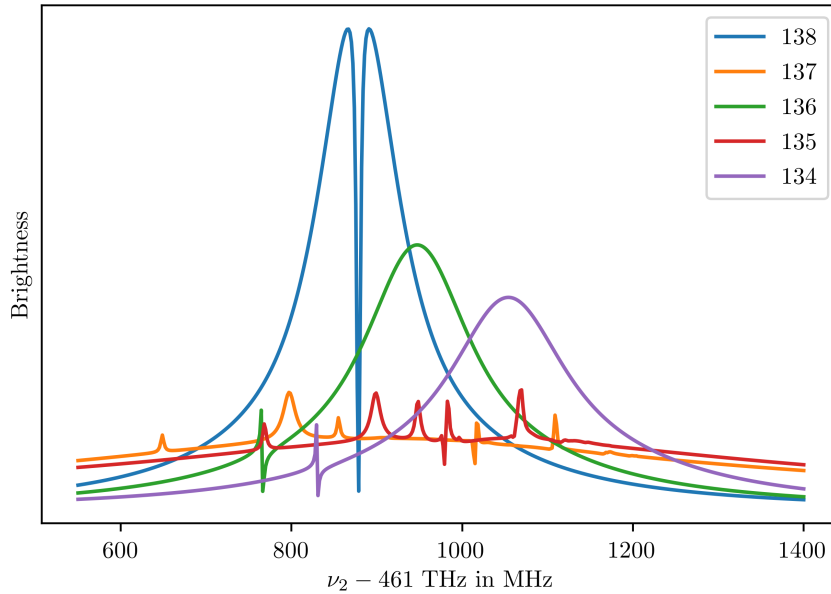


Figure 5: Simulated brightness for different isotopes of  $\text{Ba}^+$  versus  $\nu_2$ . Both laser intensities are constant at their respective saturation frequencies and  $\nu_1$  is at its resonance for  $^{138}\text{Ba}^+$ . The magnetic field is 0.1 Gauss.

One can observe that  $^{136}\text{Ba}^+$  and  $^{134}\text{Ba}^+$  behave like  $^{138}\text{Ba}^+$  – just shifted. Recall that not only is  $\nu_{\text{D-P}}$  shifted due to isotope shifts, but also  $\nu_{\text{S-P}}$ . Consequently,  $^{136}\text{Ba}^+$  and  $^{134}\text{Ba}^+$  do not simply appear as shifts of  $^{138}\text{Ba}^+$  in Figure 5 since for them  $\nu_1$  is not on resonance.

Regarding the hyperfine isotopes  $^{137}\text{Ba}^+$  and  $^{135}\text{Ba}^+$ , their fluorescence spectra appear much broader, yet also dimmer. At their respective peaks, the hyperfine isotopes are not as bright as the non-hyperfine isotopes, despite similarly large isotope shifts for the  $6s\ ^2\text{S}_{1/2} - 6p\ ^2\text{P}_{1/2}$  transition. However, further away from the peaks, the hyperfine isotopes are somewhat brighter.

In order to get a more complete picture of the brightness of the various  $\text{Ba}^+$  in dependence of the two laser frequencies I have created the plots in the subsequent sections.

### 3.4 2D Frequency Scans

Figure 6 shows the brightness for all isotopes discussed in this report ( $^{138}\text{Ba}^+$  to  $^{134}\text{Ba}^+$ ) plotted against the two laser frequencies for constant laser intensities and magnetic field.

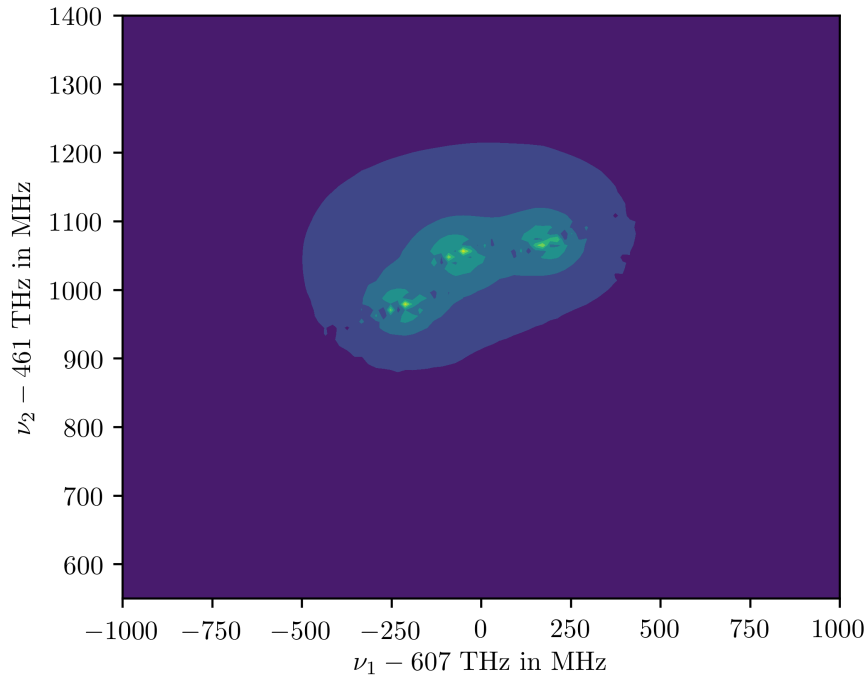


Figure 6: Simulated brightness for the isotopes  $^{138}\text{Ba}^+$  -  $^{134}\text{Ba}^+$  versus  $\nu_1$  and  $\nu_2$ . Both laser intensities are constant at their respective saturation frequencies and. The magnetic field is 5 Gauss such that the individual isotopes are more discernible.

One can clearly distinguish three peaks. These correspond to the isotopes  $^{138}\text{Ba}^+$ ,  $^{136}\text{Ba}^+$  and  $^{134}\text{Ba}^+$ , which do not experience hyperfine splitting. The isotopes  $^{137}\text{Ba}^+$  and  $^{135}\text{Ba}^+$  account for the faint, yet comparably large, blob whose shape does not match the position of the three peaks. It thus appears that the hyperfine isotopes will never be as bright as the non-hyperfine ones are on resonance. This would mean that, if one has accidentally loaded a hyperfine species of  $\text{Ba}^+$ , then no tuning of the lasers will make them bright (compared to non-hyperfine isotopes at resonance).

## 4 Ion Trap Data

In this section I will outline how I obtained data on the ions' brightness and present attempts at fitting the model to the data.

An observer can see the ions in the trap by looking through a lens. Furthermore, there is also a camera which continuously takes images through a similar lens on the reverse of the apparatus. People working on the trap can access those images in real time. To quantify the ions' brightness in the trap I used a software tool that Albert Mitjans has developed. In a first step, it determines the number and locations of ions in the trap for each image (frame) taken by the camera. In a second step, it sums over the brightness of the pixels in the vicinity of the previously determined locations of the ions and outputs the maximal value, i.e., the brightness of the brightest ion. If it cannot find any ions, it outputs zero even if summing over the pixels when the trap is empty would not yield this result.

One can control the frequencies of the two lasers via Python scripts. With the goal of reducing noise during a frequency scan I waited until the setpoint and measured frequency were close (within 10 MHz) before making use of Albert's software tool. I then took the average of ten measurements, each separated by 100 ms.

It is worth mentioning that in choosing the laser frequencies the experimenter is restricted in the sense that too high frequencies of  $\nu_1$  or  $\nu_2$  will cause the ions to heat up and escape. For  $\nu_1 > 607.426\,340$  THz and  $\nu_2 > 461.311\,940$  THz one can expect the ions to escape.

In order to change the laser intensities one has to go to the physical setup and do so manually. There is no purposefully generated magnetic field.

### 4.1 1D Frequency Scans

For 1D scans, fixing  $\nu_2$  while varying  $\nu_1$  turned out to yield better results. When scanning  $\nu_2$  the ions tended to escape more easily and the resulting graphs tended to be noisier. This made fitting the model to the data more challenging.

Figures 7 and 8 show data that I obtained by varying  $\nu_1$  and keeping  $\nu_2$  constant. The figures include fits of the model to the brightness of  $^{138}\text{Ba}^+$ . The parameters included in the model are: the magnetic field<sup>2</sup>  $B$ , the Rabi frequencies of both lasers  $\Omega_1$  and  $\Omega_2$ , the polarisation of both lasers, and an overall scaling and constant offset.

---

<sup>2</sup>Recall that the direction of the magnetic field is implicitly set along the  $z$ -axis by choosing the  $\mathbf{c}_q$  as in Equation (7). We hence fit the polarisation vectors in the coordinate system where the  $z$ -axis is the direction of the magnetic field.

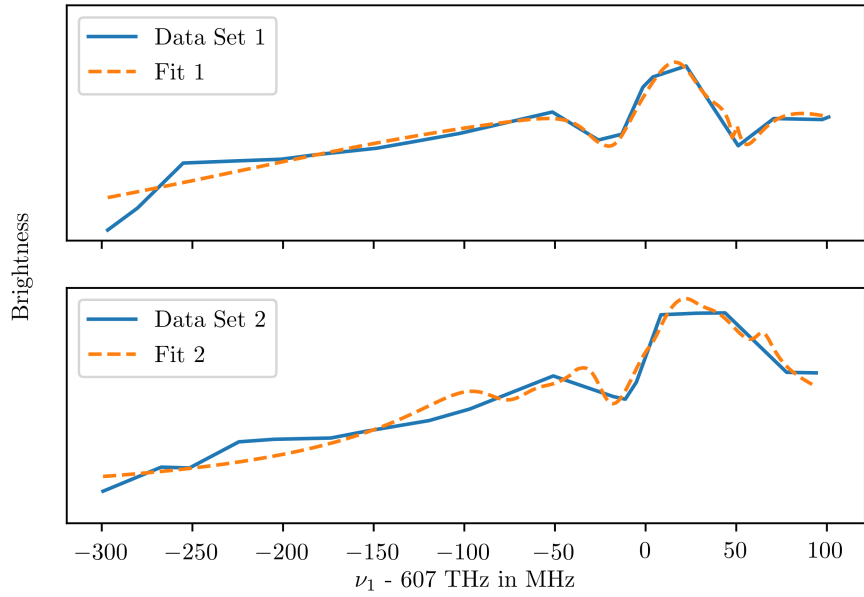


Figure 7: Measured brightness of  $\text{Ba}^+$  in the ion trap versus measured  $\nu_1$ ,  $\Delta_2 = 21.5$  MHz. Model fitted to interpolation of data. Parameters estimated by model in the first subplot:  $B = 0.43$  Gauss,  $\frac{\Omega_1}{\Omega_{1,\text{sat}}} = 31$ ,  $\frac{\Omega_2}{\Omega_{2,\text{sat}}} = 10$  and in the second subplot:  $B = 0.28$  Gauss,  $\frac{\Omega_1}{\Omega_{1,\text{sat}}} = 27$ ,  $\frac{\Omega_2}{\Omega_{2,\text{sat}}} = 16$ .

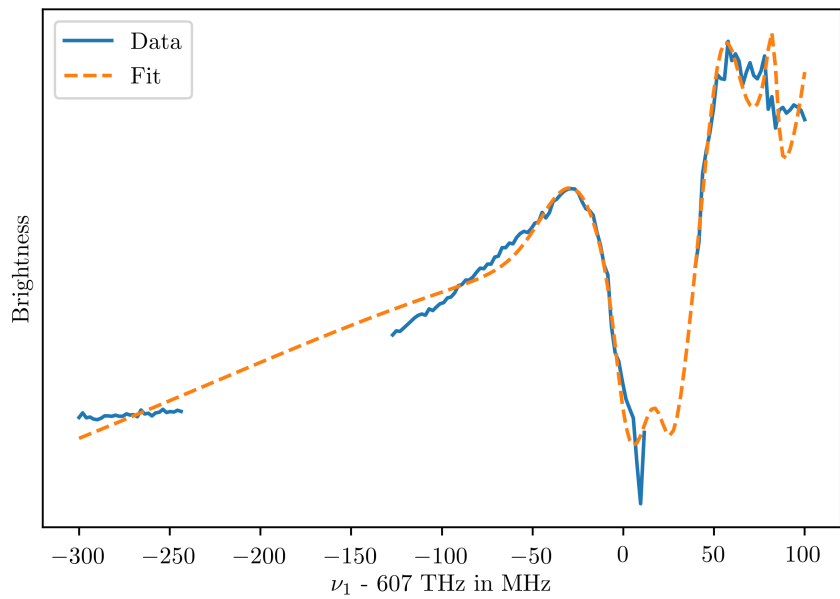


Figure 8: Measured brightness of  $\text{Ba}^+$  in the ion trap versus measured  $\nu_1$ ,  $\Delta_2 = 41.5$  MHz. Parameters estimated by model:  $B = 20$  Gauss,  $\frac{\Omega_1}{\Omega_{1,\text{sat}}} = 26$ ,  $\frac{\Omega_2}{\Omega_{2,\text{sat}}} = 6$

Apart from the fact that the model's predictions match the data qualitatively, several things are worth pointing out regarding the above figures. The gaps in the data in Figure 8 stem from how the software tool determines the brightness of the ions. If it detects no ion, zero is returned, even though summing over the pixels in the vicinity of where the ions should be would not yield this result. The gaps simply mean that the ions' fluorescence was drowned in noise in those frequency intervals and not necessarily that they were dark.

While the fitted parameters are always somewhat different, the magnetic field appears to vary significantly more than the Rabi frequencies. This might mean that the magnetic field is less relevant for the quality of the fit and the brightness of the ion.

Finally, the fit (and therefore also the quality of the fit) depends strongly on the initial guess of the solution parameters. I obtained the above results after systematically trying out different initial guesses and then using the one that resulted in the best fit. This underlines the fact that the optimisation problem the model tries to solve is highly non-convex and therefore in general not easy to solve globally.

## 4.2 2D Frequency Scans

In Section 3.4 the reader may have wondered what a 2D frequency scan as the one in Figure 6 would look like if I measure the brightness of actual ions in the trap. Reproducing Figure 6 exactly is not realistic, for two reasons. Firstly, one would have to load at least one ion of each kind of isotope of  $\text{Ba}^+$  in the trap and ensure that all of them have the same parameters (i.e. laser intensities etc.), which would be extremely hard due to the nature of the loading process and the finite waists of the laser beams. Secondly, some parts of the frequency ranges in Figure 6 would almost certainly cause the ions to escape the trap.

What I can present, however, is a 2D frequency scan of a restricted frequency window, see Figure 9 below.

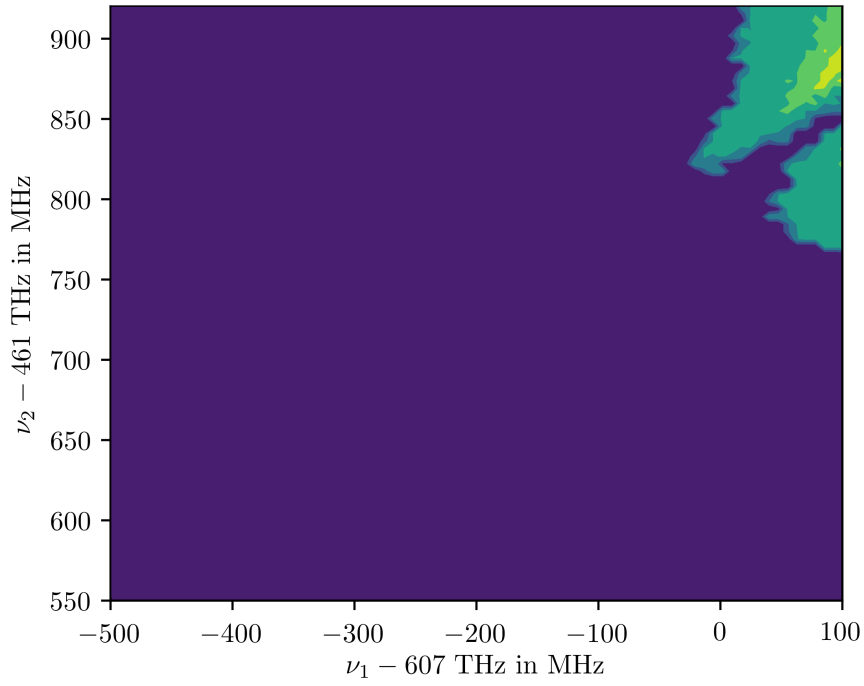


Figure 9: Measured brightness of  $\text{Ba}^+$  in the ion trap versus measured  $\nu_1$  and  $\nu_2$ .

Manually tuning the magnetic field and the Rabi frequencies, I arrived at producing a plot of the same frequency window which looks reasonably close, see Figure 10.

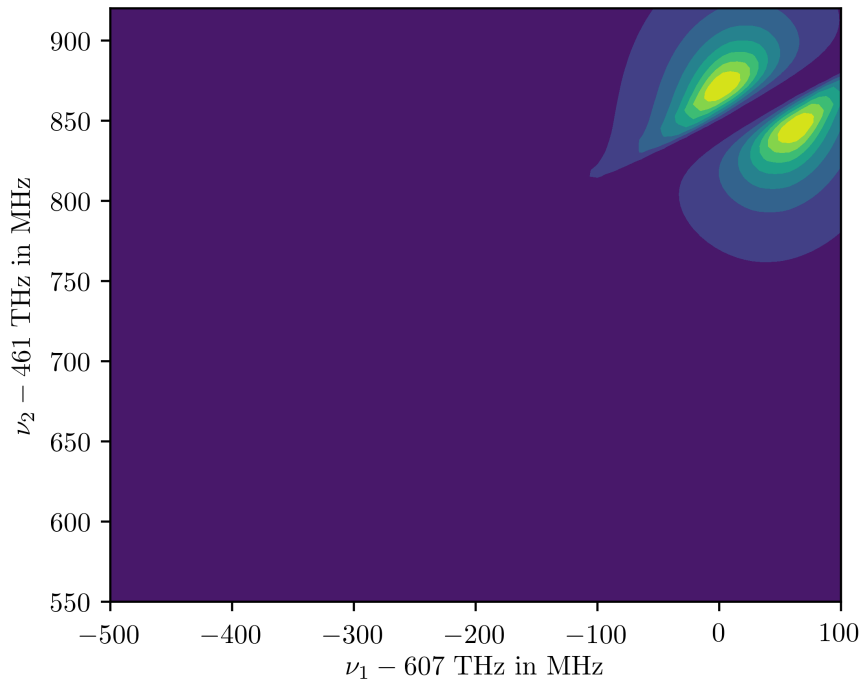


Figure 10: Simulated brightness for  $^{138}\text{Ba}^+$  versus  $\nu_1$  and  $\nu_2$ ,  $B = 5$  Gauss,  $\frac{\Omega_1}{\Omega_{1,\text{sat}}} = 2$ ,  $\frac{\Omega_2}{\Omega_{2,\text{sat}}} = 2$ .

Based on the similarity of Figures 9 and 10 it seems reasonable to guess that the ion in the trap was  $^{138}\text{Ba}^+$  as for the other isotopes the same plots look less similar as the resonances are shifted due to isotope shifts (see Table 2).

### 4.3 Intensity Dependent Brightness

The observation that some ions temporarily turn dark or dimmed does not seem to be due to either different isotopes or even molecules being in the trap, since the differences in brightness compared to  $^{138}\text{Ba}^+$  would be permanent. A possible reason for this observation is that, when several ions are in the trap, the individual ions experience different laser intensities due to the finite waists of the lasers. Below I present two graphs to illustrate the point that there are configurations of frequencies and laser intensities where a small shift in either of these quantities will result in a large change in brightness.

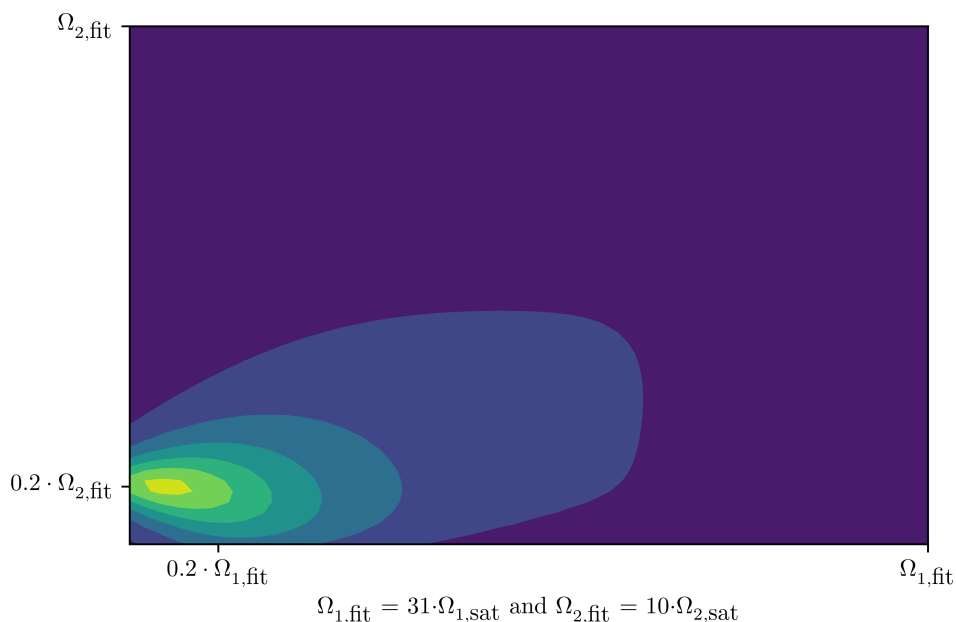


Figure 11: Simulated brightness of  $^{138}\text{Ba}^+$  versus  $\Omega_1$  and  $\Omega_2$ . The axes range from the fitted values of  $\Omega_1$  and  $\Omega_2$  from the top part of Figure 7 to 0.1 times those values. The frequencies  $\nu_1$  and  $\nu_2$  are constant such that  $\Delta_1 = 0$  and  $\Delta_2 = 21.5$  MHz,  $B = 0.43$  Gauss.

In Figure 11 the Rabi frequency configuration of the top part of Figure 7 is in the top right corner. However, in the bottom left corner there is a (small) spot where the ion would be much brighter. If we set the Rabi frequencies in the fit from the top part of Figure 7 to the values which result in the peak in the bottom left corner we get the dashed green line in Figure 12 below.

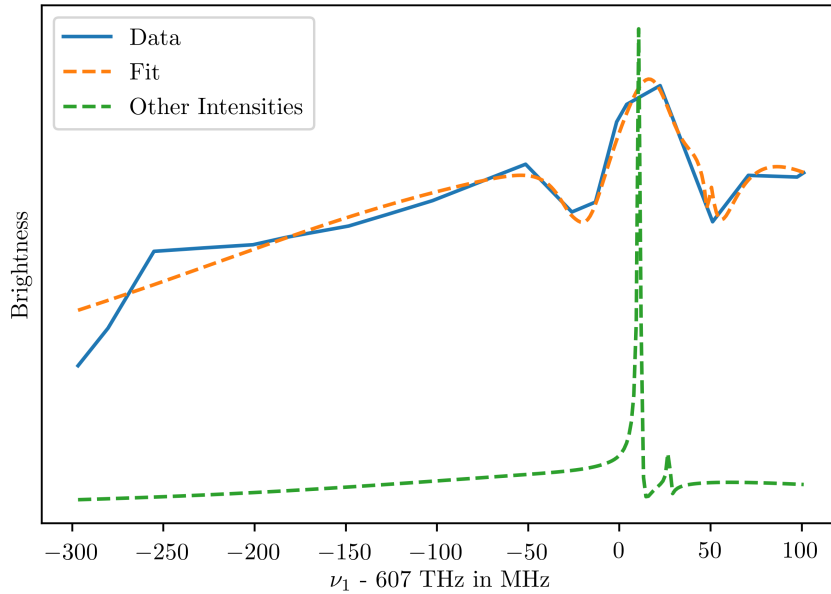


Figure 12: Measured brightness of  $\text{Ba}^+$  and fit from top part of Figure 7 as well as simulated brightness with same parameters as fit apart from the Rabi frequencies, which take on the values corresponding to the bright spot in Figure 11.

As expected, this results in a brighter ion for the value of  $\nu_1$  from Figure 11. However, this peak appears very unstable with regard to changes in  $\nu_1$ . We can conclude from Figures 11 and 12 that there are combinations of intensities and laser frequencies where the ions' brightness can change drastically when the ions experience small variations in those same parameters. It therefore seems plausible that the temporary changes in brightness of some ions is a consequence of the finite waist of the laser beams (and the motion of the ions in the trap) or fluctuations in the intensities and laser frequencies for other reasons.

How could one go about finding a more stable operating point? A potential approach is to quantify the total brightness over frequency ranges in both  $\nu_1$  and  $\nu_2$  for a given pair of Rabi frequencies, as opposed to evaluating the brightness at a single point. This way, narrow peaks as seen in Figures 11 and 12 will not stand out as much compared to broader and more stable features. To illustrate this line of thought, I have created the plot in Figure 13.

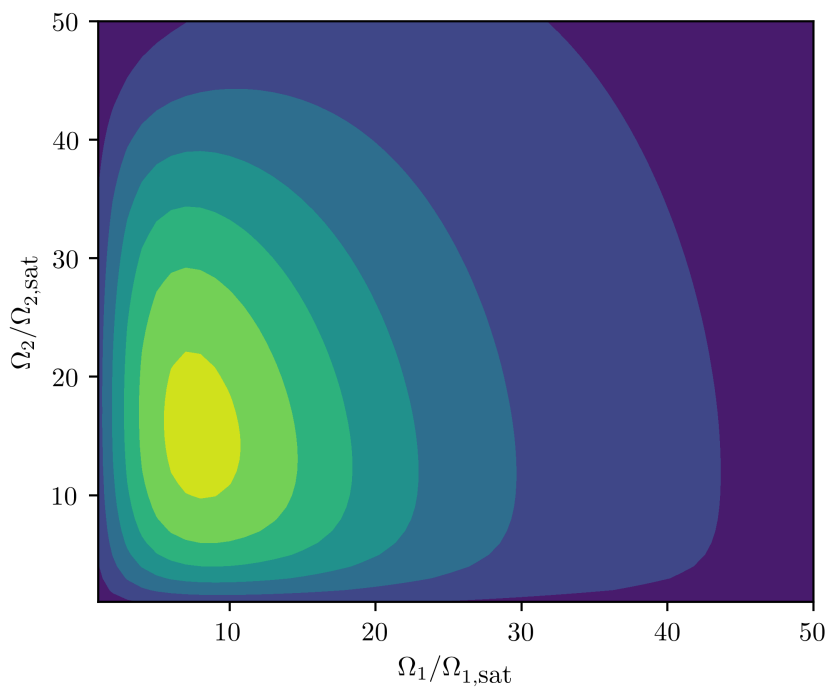


Figure 13: Simulated brightness of  $^{138}\text{Ba}^+$  versus  $\Omega_1$  and  $\Omega_2$  for  $B = 5$  Gauss. For each pair of Rabi frequencies the brightness in the graph is the total brightness (integral) over a range of 1 GHz around resonance for both  $\nu_1$  and  $\nu_2$ .

## 5 Discussion & Conclusion

In this report I discussed the construction of a model that simulates the brightness of different isotopes of  $\text{Ba}^+$  when two lasers of given frequencies, intensities and polarisations target the  $6s\ ^2S_{1/2} - 6p\ ^2P_{1/2}$  and  $5d\ ^2D_{3/2} - 6p\ ^2P_{1/2}$  transitions.

The model was able to reproduce results that previous researchers had managed to fit to their data. In a next step, the model managed to create fits to data that I obtained from our ion trap. Although the fits were qualitatively good (given reasonably un-noisy data), the estimated parameters varied somewhat from fit to fit. This was especially the case for the magnetic field. Furthermore, the quality of the solution, as well as the solution itself, depended a lot on the initial guess of the parameters. This is typical for highly non-convex optimisation problems.

What does this mean for the ion trap? For the  $\text{Ba}^+$  isotopes that experience hyperfine splitting, the model suggested that these ions would never be as bright as their non-hyperfine counterparts are on resonance. Therefore, no tuning of the lasers will make  $^{137}\text{Ba}^+$  and  $^{135}\text{Ba}^+$  as bright as  $^{138}\text{Ba}^+$  on resonance. Lest these isotopes find themselves in the trap, one could try to selectively ionise barium and selectively cool the ions in the trap. Due to the broadened lasers (see Section 3.1) this approach also does not come without its own challenges. Regarding the possibility of molecular ions forming, there was no direct evidence of this occurring.

To avoid ions becoming temporarily dark or dimmed, one should carefully choose the point of operation (i.e. the laser frequencies and intensities) carefully. Further potential future steps may include using the model to find an optimal set of working parameters and setting the laser intensities and polarisations accordingly in the physical setup.



Eidgenössische Technische Hochschule Zürich  
Swiss Federal Institute of Technology Zurich

## Declaration of originality

The signed declaration of originality is a component of every semester paper, Bachelor's thesis, Master's thesis and any other degree paper undertaken during the course of studies, including the respective electronic versions.

Lecturers may also require a declaration of originality for other written papers compiled for their courses.

---

I hereby confirm that I am the sole author of the written work here enclosed and that I have compiled it in my own words. Parts excepted are corrections of form and content by the supervisor.

**Title of work** (in block letters):

Barium Ion Cooling Simulation
-------------------------------

**Authored by** (in block letters):

*For papers written by groups the names of all authors are required.*

**Name(s):**

Mouton

**First name(s):**

Lukas

With my signature I confirm that

- I have committed none of the forms of plagiarism described in the '[Citation etiquette](#)' information sheet.
- I have documented all methods, data and processes truthfully.
- I have not manipulated any data.
- I have mentioned all persons who were significant facilitators of the work.

I am aware that the work may be screened electronically for plagiarism.

**Place, date**

Zürich, 31.05.21

**Signature(s)**

---

---

---

---

---

*For papers written by groups the names of all authors are required. Their signatures collectively guarantee the entire content of the written paper.*

## Bibliography

- [1] E. A. Dijck et al. “Determination of transition frequencies in a single  $^{138}\text{Ba}^+$  ion”. In: *Phys. Rev. A* 91 (6 June 2015), p. 060501. DOI: [10.1103/PhysRevA.91.060501](https://doi.org/10.1103/PhysRevA.91.060501). URL: <https://link.aps.org/doi/10.1103/PhysRevA.91.060501>.
- [2] J.R. Johansson, P.D. Nation, and Franco Nori. “QuTiP: An open-source Python framework for the dynamics of open quantum systems”. In: *Computer Physics Communications* 183.8 (2012), pp. 1760–1772. ISSN: 0010-4655. DOI: <https://doi.org/10.1016/j.cpc.2012.02.021>. URL: <https://www.sciencedirect.com/science/article/pii/S0010465512000835>.
- [3] J K Bowmaker and H J Dartnall. “Visual pigments of rods and cones in a human retina.” In: *The Journal of Physiology* 298.1 (1980), pp. 501–511. DOI: <https://doi.org/10.1113/jphysiol.1980.sp013097>. eprint: <https://physoc.onlinelibrary.wiley.com/doi/pdf/10.1113/jphysiol.1980.sp013097>. URL: <https://physoc.onlinelibrary.wiley.com/doi/abs/10.1113/jphysiol.1980.sp013097>.
- [4] Gillenhaal Beck. “Toward Background-Free Readout and Cooling in  $^{40}\text{Ca}^+$  with a Multiply-Connected Quadrupole Transition”. MA thesis. ETH Zürich, 2020.
- [5] Serge Haroche and Jean-Michel Raimond. *Exploring the Quantum*. Oxford University Press, 2006.
- [6] Christopher J. Foot. *Atomic Physics*. Oxford University Press, 2005.
- [7] Daniel Adam Steck. *Quantum and Atom Optics*.
- [8] Bijaya K. Sahoo et al. “Magnetic dipole hyperfine interactions in  $^{137}\text{Ba}^+$  and the accuracies of the neutral weak interaction matrix elements”. In: *Phys. Rev. A* 68 (4 Oct. 2003), p. 040501. DOI: [10.1103/PhysRevA.68.040501](https://doi.org/10.1103/PhysRevA.68.040501). URL: <https://link.aps.org/doi/10.1103/PhysRevA.68.040501>.
- [9] K. Wendt et al. “Hyperfine structure and isotope shift of the neutron-rich barium isotopes  $^{139-146}\text{Ba}$  and  $^{148}\text{Ba}$ ”. In: *Zeitschrift für Physik A Atomic Nuclei* 329.4 (1988), pp. 407–411. DOI: [10.1007/BF01294345](https://doi.org/10.1007/BF01294345). URL: <https://doi.org/10.1007/BF01294345>.
- [10] P. Villemoes et al. “Isotope shifts and hyperfine structure of  $^{134-138}\text{Ba}$  II by fast ion beam-laser spectroscopy”. In: *Journal of Physics B Atomic Molecular Physics* 26.22 (Nov. 1993), pp. 4289–4299. DOI: [10.1088/0953-4075/26/22/030](https://doi.org/10.1088/0953-4075/26/22/030).
- [11] R. E. Silverans et al. “Collinear fast beam-laser spectroscopy on  $5d^2D_{3/2,5/2}$  barium ions”. In: *Zeitschrift für Physik A Atoms and Nuclei* 295.4 (1980), pp. 311–314. DOI: [10.1007/BF01412941](https://doi.org/10.1007/BF01412941). URL: <https://doi.org/10.1007/BF01412941>.
- [12] URL: <https://www.physics.nist.gov/PhysRefData/Handbook/Tables/bariumtable1.htm>.
- [13] Phillip Ingram et al. “Collinear laser spectroscopy at ion-trap accuracy: Transition frequencies and isotope shifts in the  $6s^2S_{1/2} \rightarrow 6p^2P_{1/2,3/2}$  transitions in  $\text{Ba}^+$ ”. In: *Phys. Rev. A* 99 (1 Jan. 2019), p. 012511. DOI: [10.1103/PhysRevA.99.012511](https://doi.org/10.1103/PhysRevA.99.012511). URL: <https://link.aps.org/doi/10.1103/PhysRevA.99.012511>.
- [14] Phil Armitage. *Astrophysics I - Stellar and Interstellar, Lecture 09*. URL: <https://jila.colorado.edu/~pja/astr3730/lecture09.pdf>.

- [15] C. Nazé, J. G. Li, and M. Godefroid. “Theoretical isotope shifts in neutral barium”. In: *Phys. Rev. A* 91 (3 Mar. 2015), p. 032511. DOI: 10.1103/PhysRevA.91.032511. URL: <https://link.aps.org/doi/10.1103/PhysRevA.91.032511>.
- [16] Shannon L. Woods et al. “Dipole transition strengths in Ba<sup>+</sup> from Rydberg fine-structure measurements in Ba and Ba<sup>+</sup>”. In: *Phys. Rev. A* 82 (1 July 2010), p. 012506. DOI: 10.1103/PhysRevA.82.012506. URL: <https://link.aps.org/doi/10.1103/PhysRevA.82.012506>.
- [17] K. J. Arnold et al. “Measurements of the branching ratios for 6P<sub>1/2</sub> decays in <sup>138</sup>Ba<sup>+</sup>”. In: *Phys. Rev. A* 100 (3 Sept. 2019), p. 032503. DOI: 10.1103/PhysRevA.100.032503. URL: <https://link.aps.org/doi/10.1103/PhysRevA.100.032503>.